ELEKTROTEHNIŠKI VESTNIK 81(1-2): 51-56, 2014
ORIGINAL SCIENTIFIC PAPER

Magnetic-Field Computation of a Novel 3-DOF Deflection-Type PM Motor with Analytical and Finite-Element Methods

Zheng LI

School of Electrical Engineering, Hebei University of Science and Technology, Shijiazhuang, China
E-mail: Lzhfgd@163.com

Abstract: Based on brief introduction of the operation principle and superior performance of the permanent-magnet (PM) deflection type three-degrees-of-freedom motors, one novel PM motor air-gap magnetic-field calculation schemes based on the analytical and finite-element methods are presented and scalar magnetic-flux density calculation formulae in the spherical coordinate are developed. A rotor magnetic-field model is built in a 3D finite-element software and computed with simulation to derive the flux-density distribution under different magnetization modes. The results obtained with these two methods are compared and validated. The theoretical analysis and computation results demonstrate the effectiveness of the designed structure; it is easy for the rotor to achieve a three-degree-of-freedom deflection motion, which provides references for further research and experimental design of the related motors or actuators.

Keywords: Permanent magnet, Multi-DOF, Analytical method, Magnetic field, FEM

Izračun magnetnega polja v motorju s strajnimi magneti z analitično metodo in metodo končnih elementov

V članku je predstavljen izračun magnetnega polja v električnem motorju s trajnimi magneti. Pri izračunu smo uporabili analitično metodo in metodo končnih elementov ter predstavili izračun gostote magnetnega pretoka. Magnetno polje v rotorju smo modelirali v tridimenzionalnem prostoru in določili porazdelitev gostote magnetnega pretoka pri različnih načinih magnetizacije. Dobljene rezultate smo verificirali in primerjali. Teoretična analiza in simulacijski rezultati dokazujejo učinkovitost predlagane strukture električnega motorja s trajnimi magneti.

1 INTRODUCTION

With the development of the industry and technology, robots and manipulators, which can achieve a three-degree-of-freedom (3-DOF) motion for energy conversion, are used more and more widely. This kind of the energy-conversion devices are usually built with several conventional driver motors, each having a single degree-of-freedom, which reduces the position accuracy, efficiency and dynamic performance of the system. It is for this reason that the multi-DOF actuators or motors have attracted much attentions [1-7]. To realize the optimal structure design and precision control, an analysis method and a feedback control scheme are necessary. However, the operation mechanisms and control algorithms are not as common as those used for a single-DOF actuator control system, which are not suitable for the multi-DOF actuator applications [8]. So the analysis and control have become a crucial problem and should be paid more attention. There are mainly the analytical (magnetic circuits) and finite-element-based analysis and modeling methods for the magnetic-field calculation in actuators or motors [9]. Here, analytical and FEM softwares are selected to derive the magnetic-field characteristics for dynamic-modeling applications.

According to the original complicated 3D structure of the motor, the magnetic-field distribution and configuration-parameter determination are important in the motor design. The aim of this study is to calculate and evaluate a novel permanent-magnet deflection-type actuator by using both the analytical and 3D finite-element analysis, and to provide a detailed discussion on its distribution and characteristics. The work results can have maximum capabilities for further optimization and energy-index investigation of this kind of the motor or actuator with multiple degrees of freedom.

2 OPERATION PRINCIPLE AND STRUCTURE OF A PM MULTI-DOF ACTUATOR

The working principle of the motor is based on the interaction between the magnetic field generated by an energized coil and a PM field. A detailed description of the mechanism of the motor is given. To the 2 and 5' coils loaded DC current, it produces the magnetic poles as the N poles, and to the 2' and 5 coils loaded current produces the magnetic poles as the S poles. Its schematic diagram is shown in Fig. 1. The poles of the same polarity produce mutually exclusive forces; the magnetic poles of the opposite polarity generate attractive forces, that derive a synthesized electromagnetic torque making the rotor complete the

Received 11 January 2014
Accepted 27 February 2014

movement around the X-axis deflection. Fig. 1 also gives a schematic cross-sectional view of the movement around the X-axis deflection.

Activating the 3, 4, 1' and 6' coils with the load currents produces the magnetic poles of the S-polarity; the magnetic poles generated by the 3', 4', 1 and 6 coils with the load current produce the poles of the N-polarity. Thus, the synthetic electromagnetic torque is exerted on the motor rotor to do a yaw movement around the Y axis. The schematic diagram is shown in Fig. 2.

Activating the 1, 1', 4 and 4' coils with the load currents produces the magnetic poles of the S-polarity; activating the 3, 3', 6 and 6' coils with the load currents produces the magnetic poles of the N-polarity. The magnetic S-poles generated by the currents produce tangential tensile components on the PM rotor N-poles, and the current generation of the N-poles causes tangential thrust components of the PM rotor N-poles. The synthetic tangential electromagnetic torques turn the actuator into a rotational movement around the Z-axis. Because of the different positions of the actuator's rotor, inducing a special current through the current controller of the corresponding coil, a successive Z-axis rotational motions of the actuator can be realized. Fig. 3 shows a schematic diagram of the motor around the Z-axis rotation.

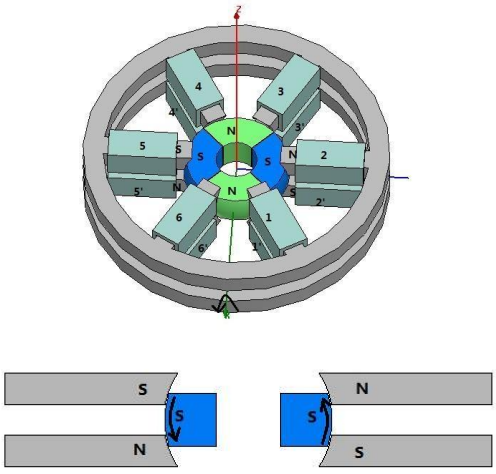

Figure 1. Deflection-type motion around the X axis

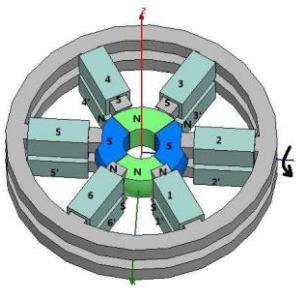

Figure 2. Deflection-type motion around the Y axis

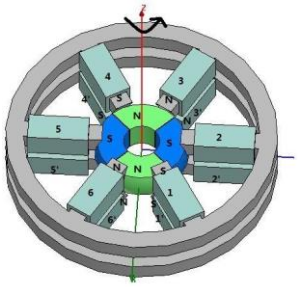

Figure 3. Deflection-type motion around the Z axis

The three-degree-of-freedom actuator structure limits the deflection motions around the X and Y axes to a certain angle. By changing the direction of the energized current in the coil, the motor can be realized by the reverse direction movement.

3 Analytical Analysis of the Actuator

3.1 Classification of the magnetic-field solution area

The electromagnetic-field analysis plays an important role in the calculation of the design and parameters of the PM motor. An analytical analysis of the electromagnetic-field results, and of physical concepts contribute to optimisation of the qualitative aspects of the relationship between the magnetic-field distribution of the main structure of the motor parameters and can be intuitively drawn. As the magnetic field generated by the magnetic pole of the PM rotor is an important part of the air-gap magnetic field, it is necessary to analyze the PM rotot-pole magnetic-field. Table 1 shows the main parameters of the PM rotor.

The magnetic field produced by the PM rotor can be divided into 2 parts [8, 10]:

the outer magnetic field of the rotor, with the magnetization characteristics

$$B_1 = \mu_0 H_1 \tag{1}$$

where μ_0 is the permeability of vacuum, $\mu_0 = 4\pi \times 10^{-7}\,\mathrm{H}/m$, and

the inner magnetic field of the rotor, with the magnetization characteristics

$$B_2 = \mu_0 \mu_r H_2 + \mu_0 M_0 \tag{2}$$

where μ_r is the PM relative magnetic permeability, M_0 is the residual magnetization, $M_0 = B_{rem} / \mu_0$, B_{rem} is the residual magnetic-flux density.

From (1) and (2), it follows

$$\nabla \times H_k = 0, k = 1,2 \tag{3}$$

$$\nabla \times B_k = 0, k = 1,2 \tag{4}$$

H_k can be expressed by the scalar magnetic potential Φ_k gradient as

$$H_k = -\nabla\Phi_k \tag{5}$$

Thus, the followings can be derived from the above formula

$$\nabla^2\Phi_1 = 0 \tag{6}$$

$$\nabla^2\Phi_2 = 1/\mu_0 \nabla\cdot M_0 = 0 \tag{7}$$

3.2 Scalar magnetic-potential general solution

The magnetic field of the PM rotor of the motor can be reduced to solving problems with the Laplace equation under certain boundary conditions. The Laplace equation in spherical coordinates is:

$$\frac{1}{r^2}\left[\frac{\partial}{\partial r}(r^2\Phi_i) + \frac{1}{\sin\theta}\frac{\partial}{\partial\theta}(\sin\theta\frac{\partial\Phi_i}{\partial\theta}) + \frac{1}{\sin^2\theta}\frac{\partial\Phi_i}{\partial\varphi}\right] = 0 \tag{8}$$

The scalar magnetic potential in the spherical coordinate's Laplace general solution is

$$\Phi_i = \sum_{n=0}^{\infty}\sum_{m=-n}^{n}(k_{n,i}^m r^n + \varepsilon_{n,i}^m r^{-(n+1)})Y_n^m(\theta,\varphi) \tag{9}$$

Outside diameter	Inner diameter	Latitude angle	Pole pairs
Rr/mm	Rb/mm	β/°	P
15.5	5	36	2
Residual magnetic-flux density	Relative magnetic permeability	Distance to the rotor centre	Residual magnetic-flux density
B_r / T	μ_r	d/mm	B_r / T
1.14	1.02	15.7	1.14

where i=1, 2 represents the two parts of the magnetic field, and $k_{n,i}^m$ and $\varepsilon_{n,i}^m$ are determined by the boundary conditions.

$$Y_n^m(\theta,\varphi) = S_n^m P_n^m(\cos\theta)e^{im\varphi} \tag{10}$$

where $S_n^m = \sqrt{\frac{(2n+1)(n-m)!}{4\pi(n+m)!}}$, $P_n^m(\cos\theta)$ denotes the Legendre functions, and

$$P_n^m(\cos\theta) = \frac{1}{2^n n!}(1-\cos^2\theta)^{\frac{m}{2}}\frac{d^{m+n}}{dx^{m+n}}(\cos^2\theta-1)^n \tag{11}$$

Table 1: The parameters of the PM rotor in computation

3.3 Air-gap magnetic-field density

Based on the scalar magnetic-potential general solution, the air-gap magnetic field density B_1 can be expressed with equation (12).

$$\mathrm{B}_1 = \begin{bmatrix}\mathrm{B}_{1\gamma}\\ \mathrm{B}_{1\theta}\\ \mathrm{B}_{1\varphi}\end{bmatrix} = \begin{bmatrix}\sum_{n=2,4,\ldots}^{\infty}\sum_{m=\pm2,\pm10,\ldots}^{\pm n}((n+1)\mu_r\varepsilon_n^m\frac{1}{r^{n+2}})Y_n^m(\theta,\varphi)\\ \sum_{n=2,4,\ldots}^{\infty}\sum_{m=\pm2,\pm10,\ldots}^{\pm n}(-\mu_r\varepsilon_n^m\frac{1}{r^{n+2}})\frac{\partial Y_n^m(\theta,\varphi)}{\partial\theta}\\ \sum_{n=2,4,\ldots}^{\infty}\sum_{m=\pm2,\pm10,\ldots}^{\pm n}(-\mu_r\varepsilon_n^m\frac{1}{r^{n+2}})\frac{1}{\sin\theta}\frac{\partial Y_n^m(\theta,\varphi)}{\partial\varphi}\end{bmatrix} \tag{12}$$

Then B_1 can be further calculated from the boundary conditions of the PM motor, $k_{n,1}^m = o_{n,5}C_{nm}$ and $\varepsilon_{n,1}^m = o_{n,6}C_{nm}$, where R_s is the inner diameter of the stator.

$$o_{n,6} = -(o_{n,3}/o_{n,4}R_r^{2n+1} - o_{n,2}/o_{n,1})/(R_r^{2n+1} - R_s^{2n+1})R_s^{2n+1}$$

$$o_{n,5} = (o_{n,3}/o_{n,4}R_r^{2n+1} - o_{n,2}/o_{n,1})/(R_r^{2n+1} - R_s^{2n+1})$$

$$o_{n,4} = [(\mu_r - \mu_m)nR_b^{2n+1}]$$

$$O_{n,3} = [\mu_r n + \mu_m(n+1)]O_{n,2}/O_{n,1} - R_b^{n+2}\{nR_r^{2n+1}(1-\mu_m) + (n+1+\mu_m n)R_s^{2n+1}\}$$

$$O_{n,2} = R_r^{n+2}(R_r^{2n+1} - R_s^{2n+1})(\mu_r - \mu_m)nR_b^{2n+1} - R_b^{n+2}R_r^{2n+1}\cdot\{nR_r^{2n+1}(1-\mu_m) + (n+1+\mu_m n)R_s^{2n+1}\}$$

$$o_{n,1} = \{[n+\mu_m(n+1)]R_r^{2n+1} + [(n+1)-\mu_m(n+1)]R_s^{2n+1}\}(\mu_r - \mu_m)nR_b^{2n+1} - R_r^{2n+1}\{nR_r^{2n+1}(1-\mu_m) + (n+1+\mu_m n)R_s^{2n+1}\}[\mu_r n + \mu_m(n+1)]$$

and from

$$C_{nm} = M_0\int_0^{2\pi} f(\varphi)e^{-im\varphi}d\varphi\int_0^{\pi} S_n^m\left[P_n^m(\cos\theta)\right]\sin^2\theta d\theta \tag{13}$$

where

$$f(\phi) = (-1)^{p-1}\cos[\phi - \alpha_0 - \frac{\pi}{4}(p-1)],\ p=1,2,\cdots\cdots 8$$

When n=2, it is the fundamental component of the flux density with the θ direction. The fundamental component of the air-gap flux density can be derived by the fundamental magnetic potential:

$$\begin{bmatrix}B_{11r}\\ B_{11\theta}\\ B_{11\varphi}\end{bmatrix} = \begin{bmatrix}\frac{2.3184a_2c_{22}|B_r|R_r^4(-5R_rR_b^4\mu_r + 3R_r^5\mu_r + 2R_r^5\mu_m + 2R_b^5\mu_r - 2R_b^5\mu_m)}{-6R_b^5\mu_m + 6R_b^5\mu_r\mu_m + 6R_b^5\mu_r - 6R_b^5\mu_r^2 + 4R_r^5\mu_r\mu_m + 6R_r^5\mu_m + 9R_r^5\mu_r + 6\mu_r^2R_r^5}r^{-4}\cos2\varphi\sin^2\theta\\ \frac{-0.7728a_2c_{22}|B_r|R_r^4(-5R_rR_b^4\mu_r + 3R_r^5\mu_r + 2R_r^5\mu_m + 2R_b^5\mu_r - 2R_b^5\mu_m)}{-6R_b^5\mu_m + 6R_b^5\mu_r\mu_m + 6R_b^5\mu_r - 6R_b^5\mu_r^2 + 4R_r^5\mu_r\mu_m + 6R_r^5\mu_m + 9R_r^5\mu_r + 6\mu_r^2R_r^5}r^{-4}\cos2\varphi\sin\theta\\ \frac{1.5456a_2c_{22}|B_r|R_r^4(-5R_rR_b^4\mu_r + 3R_r^5\mu_r + 2R_r^5\mu_m + 2R_b^5\mu_r - 2R_b^5\mu_m)}{-6R_b^5\mu_m + 6R_b^5\mu_r\mu_m + 6R_b^5\mu_r - 6R_b^5\mu_r^2 + 4R_r^5\mu_r\mu_m + 6R_r^5\mu_m + 9R_r^5\mu_r + 6\mu_r^2R_r^5}r^{-4}\sin2\varphi\sin\theta\end{bmatrix} \tag{14}$$

When m=n=2,

$$B_{11r} = \frac{2.3184a_2c_{22}|B_r|R_r^4(-5R_rR_b\mu_r + 3R_r^5\mu_r + 2R_r^5\mu_m + 2R_b^5\mu_r - 2R_b^5\mu_m)}{-6R_b^5\mu_m + 6R_b^5\mu_r\mu_m + 6R_b^5\mu_r - 6R_b^5\mu_r^2 + 4R_b^5R_b\mu_r\mu_m + 6R_r^5\mu_m + 9R_r^5\mu_r + 6R_r^5\mu_r^2}\cdot r^{-4}\cos2\varphi\sin^2\theta$$

Taking the harmonics of the magnetic field along the ϕ and θ directions into account, the surface of B_{11r} with the changes in ϕ and θ can be derived as shown in Fig. 5.

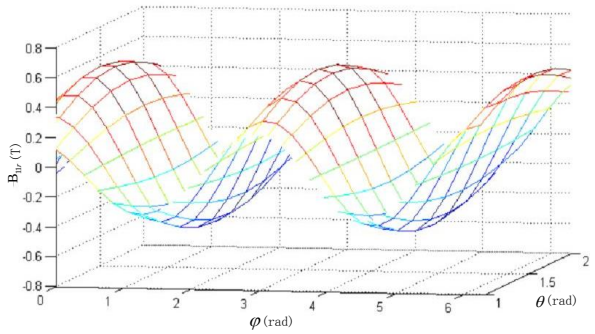

Figure 5. B_{11r} distribution of the drum-type rotor

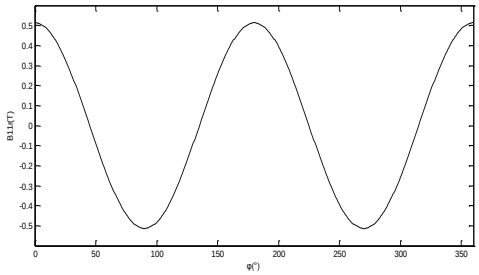

Figure 6. Changes in B_{11r} with ϕ

As seen from Fig. 5, B_{11r} changes with ϕ and θ in the form of the cosine-wave surfaces, having the peak points of the two positive and two negative peak points along the equator, which is consistent with the four-pole structure of the drum-shaped rotor magnet. When $\theta=\pi/2$, the variation of B_{11r} is shown in figure 6. As shown in Fig. 6, when θ is fixed, the fundamental wave component in the ϕ direction of the B_{11r} varies sinusoidally. The distance between the two peaks is 180 °, the peak value is 0.5135T and the electrical angle is of twice the mechanical angle.

4 Finite-Element Analysis of the PM Rotor Magnetic Field

4.1 Geometric and material parameters of the PM rotor

The finite-element model of the PM rotor is shown in Fig. 7. The overall structure of rotor takes the drum shape. For the drum-type rotor, the ball radius is R=15.5mm, the rotor thickness is 10mm, the cylinder of the radius of 5mm is in the central position where placed the output shaft; the rotor has two pairs of the magnetic poles, the N poles and the S poles that are alternately arranged around the Z axis with the pole pitch of 0.2mm.

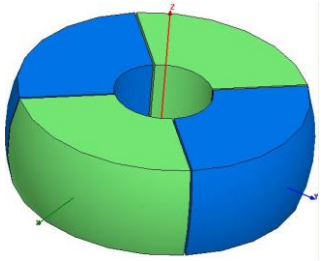

Figure 7. PM rotor model

To calculate PMs, there are usually two current-simulation methods used: the body current-density analog and the surface current-density analog. The linear PM generally equals the currents on its surface. The linear PM material relational expression is

$$M_p = \mu_r \times H_c \tag{16}$$

where M_p is the PM magnetization intensity, μ_r is the relative magnetic permeability, H_c is the ferromagnetic material coercivity.

$$B_r = \mu_0 \times M_p \tag{17}$$

This means that among parameters M_p, μ_r, H_c and B_r, only two are independent from each other. To define the linear PM material, two parameters are needed. They can be calculated based on the relationship. In one case, the *NdFeB* PM material is selected for the motor rotor, with PM relative permeability μ_r of 1.02, and coercive force H_c of -890kA/m. The calculated PM polarization is 907.8kA/m and the residual magnetic-flux density is 1.14T.

4.2 PM Magnetizing forms

The magnetizing modes of the motor PM rotor can be the radial, the axial and the parallel three-way magnetization. The radial magnetization is in a spherical coordinate system. The center of the ball drum is talken as the starting point, extending the magnet magnetization direction along the R axis; the axial magnetization is in a cylindrical coordinate system, taking Z axis as the axis, and the magnet magnetization direction is along the ρ axis; the parallel magnetization is in the space of the Cartesian coordinate system, the magnetization direction of the magnet is along a certain coordinate axis, and the magnetization direction is perpendicular to the plane formed by the other two axes along the coordinate-axis direction. It follows that by taking a single PM pole, the N pole for example, the vector distribution of the magnetic-flux density with three magnetizing ways is given as shown in Figs. 8-10.

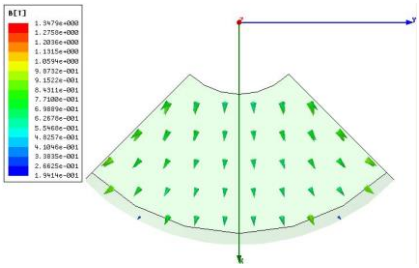

Figure 8. Radial magnetization mode

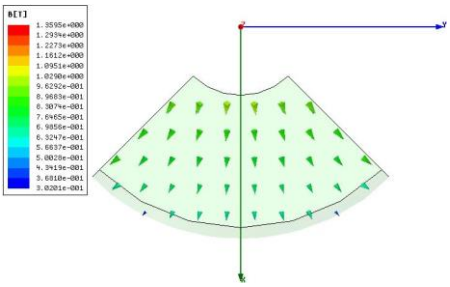

Figure 9. Axial magnetization mode

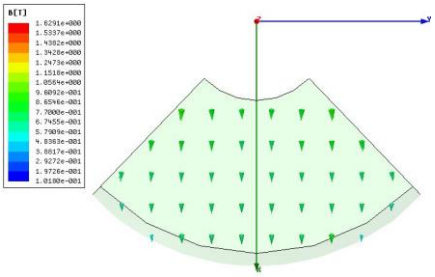

Figure 10. Parallel magnetization mode

4.3 FEM analysis on the rotor magnetic field

The finite-element analysis software Ansoft Maxwell 3D module is used to model and calculate the magnetic-field. The following axial magnetization is taken as an example to analyze the magnetic field generated by the rotor PM in the axial magnetization mode. The motor PM rotor flux-density vector distributions are shown in Figs. 11-12.

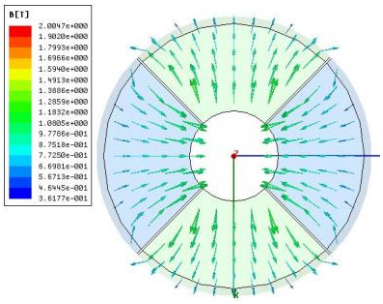

Figure 11. Flux-density vector

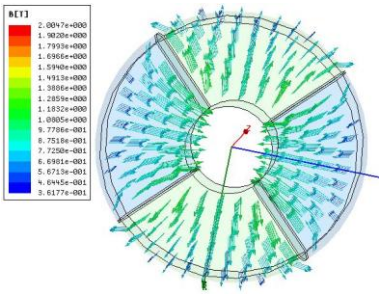

Figure 12. 3D flux-density vector

In the motor PM rotor equatorial 0.2mm circumferential path (the starting point to the intersection with the X axis, the direction is counter-clockwise), that is, in the spherical coordinate position of θ=90°, the modulus value of the magnetic intensity calculated curve is shown in Fig. 13. A comparison with the fundamental amplitude of Fig. 5 shows that the data obtained with the two methods are basically identical. In the peak position and on the amplitude level, they are more consistent, but they fully verify the correctness of the magnetic-field computational analysis and for a similar spherical PM.

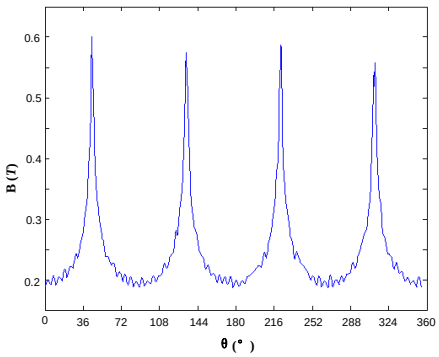

Figure 13. Flux density magnitude values of φ=90°

5 CONCLUSION

Based on a new type of the multi-degree-of-freedom PM motor structure proposed in this paper, an air-gap magnetic-field calculation and analysis methods of the PM rotor and analysis methods are explored, for other with an analytic method and a three-dimensional finite-element method. Results of the calculations, analysis and comparison of the magnetization flux-density distribution in the radial and axial directions are given, providing the bases to calculate the torque of the motor rotation and yaw movements. The calculation results verify the effectiveness of the design and give the references for further design and optimization of the 3-DOF deflection-type PM motor. PM stator and rotor-structure parameter optimization and control-strategy design are the next step of our future work.

ACKNOWLEDGMENTS

This work is supported by the National Natural Science Foundation of China (No. 51107031), the Natural Science Foundation of Hebei Province of China (No. E2014208134), the Foundation of China Scholarship Council.

REFERENCES

[1] Gregory S Chirikjian, David Stein. "Kinematic design and commutation of a spherical stepper motor". *IEEE Trans. on Mechatronics*, 4, 4(1999), pp. 342–353.

[2] David Stein, Gregory S Chirikjian. "Experiments in the Commutation and Motion Planning of a Spherical Stepper Motor". *ASME Design Engineering Technical Conferences and Computers and Information in Engineering Conference*, / Baltimore, Maryland, 2000, pp. 1-7.

[3] Davey K, Vachtsevanos G,Powers R. "The analysis of fields and torques in spherical induction motors". *IEEE Trans. on Magn*etics, 23, 1(1987), pp. 273–282.

[4] Raye A, Kok-Meng Lee. "Finite Element Torque Modeling for the Design of a Spherical Motor". *In Proc. the 7th Int. Conf. on Control, Automation and Robotics and Vision*, Singapore, 2002, pp. 390-395.

[5] J. Wang, G. W. Jewell, D. Howe. "Analysis, design and control of a novel spherical permanent-magnet actuator". *IEE Proc. Electric Power Applications*. 145, 1(1998), pp.61–71.

[6] B. Dehez, G. Galary, D. Grenier, B. Raucent. "Development of a Spherical Induction Motor with Two Degrees of Freedom". *IEEE Trans. on Magnetics*, 42, 8(2006), pp. 2077–2089.

[7] Wang Qunjing, Li Zheng, Xia Kun, Ni Youyuan. "Calculation and Analysis on Configuration Parameters and Torque Characteristics of a Novel Spherical Stepper Motor". *Proceedings of the CSEE*, 26, 10(2006), pp. 58–165.

[8] Zheng LI. "Robust control of PM spherical stepper motor based on neural networks". *IEEE Transactions on Industrial Electronics*, 56, 8 (2009), pp. 2945-2954.

[9] Zheng Li, Huiqin Sun, Xueli Wu and Qingrui Liu. "Modeling and levitation control of a novel M-DOF actuator based on neural network". *International Journal of Applied Electromagnetics and Mechanics*, 38, 2(2012), pp. 217-230.

[10] Zheng Li, Yongtao Wang, "Finite Element Analysis and Structural Optimization of a Permanent Magnet Spherical Actuator". *Electronics and Electrical Engineering*, 114, 8(2011), pp. 67-72.

Zheng LI received his B.Sc. and Ph.D. degrees in electrical engineering and power electronics and electric drive from Hefei University of Technology, Hefei, China, in 2002 and 2007, respectively. Since 2007, he has been a Lecturer, Associate Professor and Professor with the School of Electrical Engineering, Hebei University of Science and Technology. He is the author of more than 70 published papers. His current research interests include design, analysis, and control of novel motors and actuators, intelligent control, and power electronics. He is an active reviewer for the IEEE Transactions on Industrial Electronics, IEEE Transactions on Energy Conversion, IEEE Transactions on Magnetics and Electric Power Components and Systems, etc.